Universal Cyclic Topology in Polymer Networks

Rui Wang,[1] Alfredo Alexander-Katz,[2] Jeremiah A. Johnson,[3,*] and Bradley D. Olsen[1,†]
[1]Department of Chemical Engineering, Massachusetts Institute of Technology, Cambridge, Massachusetts 02139, USA
[2]Department of Material Science and Engineering, Massachusetts Institute of Technology, Cambridge, Massachusetts 02139, USA
[3]Department of Chemistry, Massachusetts Institute of Technology, Cambridge, Massachusetts 02139, USA
(Received 11 November 2015; revised manuscript received 4 February 2016; published 5 May 2016)

Polymer networks invariably possess topological defects: loops of different orders which have profound effects on network properties. Here, we demonstrate that all cyclic topologies are a universal function of a single dimensionless parameter characterizing the conditions for network formation. The theory is in excellent agreement with both experimental measurements of hydrogel loop fractions and Monte Carlo simulations without any fitting parameters. We demonstrate the superposition of the dilution effect and chain-length effect on loop formation. The one-to-one correspondence between the network topology and primary loop fraction demonstrates that the entire network topology is characterized by measurement of just primary loops, a single chain topological feature. Different cyclic defects cannot vary independently, in contrast to the intuition that the densities of all topological species are freely adjustable. Quantifying these defects facilitates studying the correlations between the topology and properties of polymer networks, providing a key step in overcoming an outstanding challenge in polymer physics.

DOI: 10.1103/PhysRevLett.116.188302

Polymer networks are widely used for applications ranging from commodity materials [1–4], such as superabsorbers, selective membranes, and high-impact rubbers, to biomedical materials, such as drug delivery devices, tissue engineering scaffolds, and extracellular matrix [5–14]. However, effectively characterizing the structure of polymer networks and understanding the correlation between the topology and properties remains an outstanding challenge. Much of our fundamental knowledge about polymer networks is based on homogeneous acyclic treelike structures [1,15–21]. Although the spatial inhomogeneity in polymer networks can be reduced by end-linking of precursor chains via f-functional junctions [22] [Fig. 1(a)], all polymer networks inevitably possess topological defects: loops [Fig. 1(b)] formed by intrinsic intramolecular reactions. These cyclic defects weaken the materials depending upon the type of loop structure formed: primary loops are completely elastically inactive, while higher-order loops may contribute to elasticity differently depending upon their specific topology. Our inability to quantify these aspects of network structure hinders our ability to quantitatively predict the mechanical response of polymer networks. For example, a systematic treatment of loop structure is essential for testing the validity of the affine and phantom network models in real polymer networks, a long-standing problem in polymer science [15]. Beyond polymer networks, cyclic defects suppressing the spread of information also exist in many other networks [23,24], such as routing loops in computer networks and acquaintance clusters in social networks. Therefore, understanding and controlling cyclic defects is critical to many forms of network science and engineering.

Theoretical efforts have addressed the delay of the gel point due to loop formation [25–28]; however, the intrinsic dependence of the cyclic topology on the condition under which the polymer network is formed as well as the inherent relations between different orders of loop structures are unknown [29,30]. Experimental techniques such as rheology or spectroscopy and multiple-quantum NMR can provide semiquantitative information related to the loop structure [31–33]. Recently, Zhou *et al.* reported "network disassembly spectrometry" (NDS), which is the first experimental method for directly quantifying primary loops [34,35]. A theory that can fully describe the dilution and chain-length effects on primary loop fraction observed in experiments is lacking. Previous theoretical work needs to use different fitting parameters for the same polymer as chain length varies [35]. Moreover, recent experimental results show that the modulus of real networks deviates

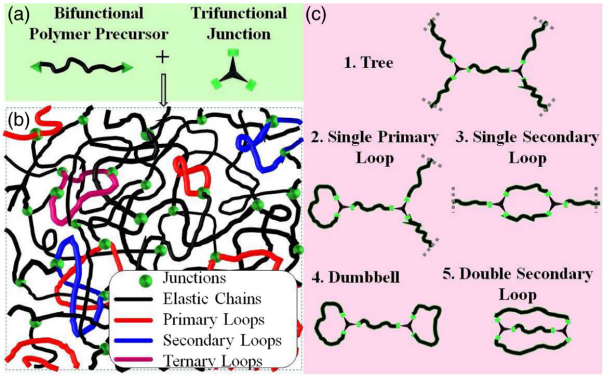

FIG. 1. Schematic of end-linked polymer networks. (a) General end-linking reaction between a bifunctional polymer precursor (A_2) and a trifunctional junction (B_3). (b) Schematic of a network with different orders of cyclic defects. (c) An exhaustive list of subgraphs considered in the modified rate theory for stoichiometric end-linking at full conversion.

significantly from ideal network models, even though the primary loop effect has been either eliminated by designing the precursors [36] or corrected through subtracting the wasted strands measured by NDS [37]. This discrepancy demonstrates the pronounced role of higher-order loops not captured by previous theories. While the effect of primary loops on network mechanics is well understood, the elastic effectiveness of polymer strands in higher-order loops is unknown. Therefore, it is desirable to understand higher-order topologies within polymer networks, so that the impacts of different cyclic defects on network properties can be decoupled and quantified separately.

Here we consider a network prepared via end-linking bifunctional (A_2) polymer precursors and trifunctional (B_3) junctions [Fig. 1(a)]. To describe both the topology of polymer networks and the kinetics of network formation, we develop a modified rate theory based on the work of Stepto and co-workers [38–40], which is a kinetic graph theory using a set of finite number of subgraphs to represent the unmanageably large network. The formation and interconversion of different subgraphs is tracked through a coupled system of differential equations. Here, subgraphs are restricted to a critical size of two nodes; cyclic topologies formed within the critical size are recorded (see Sec. I of Supplemental Material for the list of all 42 subgraphs considered for the $A_2 + B_3$ system [41]). Each functional group on the junction may be unreacted, contain a dangling chain, contain a looped chain, or be connected to the network through a bridging chain. Beyond the critical size, junctions are assumed to be uncorrelated, which can randomly react with each other. For functional groups belonging to different subgraphs, the rate for forming the bridge connecting these two subgraphs is given by

$$R_{ij,\mathrm{bridge}} = k_{AB}[A_i][B_j], \tag{1}$$

where k_{AB} is the second-order rate constant and $[A_i]$ and $[B_j]$ are the instantaneous concentrations of A and B functional groups on species i and j, respectively. Since the initial polymer concentrations for all experimental data to be described in this work are beyond the dilute polymer solution regime, the polymer precursor A_2 is modeled as a monodispersed flexible Gaussian chain. In this case, the rate of forming an intramolecular loop depends upon the probability of the two ends of an nth-order chain encountering each other, $P_n = (3/2\pi n\langle R^2\rangle)^{3/2}$. $\langle R^2\rangle = (M/m)b^2$ is the mean-square end-to-end distance of polymers which can be estimated from the molar mass of A_2 (M), the published values of Kuhn length (b), and the molar mass of a Kuhn monomer (m). Hence, for groups belonging to the same subgraph, the rate of forming the intramolecular loop is given by

$$R_{i,\mathrm{loop}} = k_{AB}\frac{N_{A,i}^n}{N_{\mathrm{Av}}}\left(\frac{3}{2\pi n\langle R^2\rangle}\right)^{3/2}[B_i], \tag{2}$$

where $N_{A,i}^n$ is the number of functional group A contained in subgraph i which can form the nth-order loop, and N_{Av} is Avogadro's number. This theory can be easily generalized to polymer precursors with other chain statistics, such as semiflexible polymers [43], by reevaluating the probability density for closing the loop in the corresponding chain statistics [44], and to polymer network systems with different junction functionalities or disperse chain lengths. Furthermore, the theory can also be applied to study the formation and the structure of cyclic defects in other types of networks [23,24].

Compared to previous work that focused only on a single junction, this work expands the set of subgraphs to all possible configurations containing two junctions [see Fig. 1(c) for subgraphs present in stoichiometric end-linking at full conversion]. Increasing the critical size of subgraphs enables a more accurate description of local correlations between junctions and allows simultaneous quantification of both primary and higher-order loops.

Comparison between the two junction rate theory and experimental measurements of loops in polymer networks shows quantitative agreement between theory and experiment with no variable parameters. Loop fractions f_n (the fraction of all junctions contained in one nth-order loop) predicted by the two junction theory are compared to the published NDS experimental data [35] for poly(ethylene glycol) (PEG) networks and the Monte Carlo (MC) simulations (see Sec. II of Supplemental Material for a description of the MC algorithm [41]). The order of a loop is defined as the number of chains required to close the loop [Fig. 1(c)]. Figure 2 plots loop fractions f_n versus the initial polymer molar concentration (c) concentration for PEG precursors with three different chain lengths [45]. As shown in Fig. 2(a), the primary loop fraction predicted by our theory is in excellent agreement with both the experimental data and MC simulations. Using intrinsic parameters of PEG reported in the literature [15] (Kuhn length $b = 1.1$ nm and molar mass of Kuhn monomer $m = 137$ g/mol), the two junction theory can quantitatively describe both the dilution and chain-length effects on the primary loop fraction; this is superior to previous work that used the Kuhn segment length as a fitting parameter, resulting in discrepancies as chain length was varied [35].

The two junction theory is also able to predict the secondary loop fraction f_2 [Fig. 2(b)], which cannot yet be quantified experimentally. Unlike the monotonic decay of f_1, the concentration dependence of f_2 presents a maximum with the same peak value for different PEG precursors. The secondary loop fraction predicted by the theory is in good agreement with the MC simulations (especially for longer PEG) in the entire concentration region except the neighborhood of the maximum, because intramolecular correlations beyond two junctions, which are accounted for in the MC simulation, are assumed to be absent in the theory.

A dimensional analysis shows that cyclic defects depend on a single universal parameter characterizing the formation condition of networks. For stoichiometric end-linking at full conversion, as the cases studied in Fig. 2, the dimensionless loop fractions f_n must be uniquely determined by the dimensionless variable $c\langle R^2\rangle^{3/2} = cb^3(M/m)^{3/2}$ that diminishes the volume unit. This

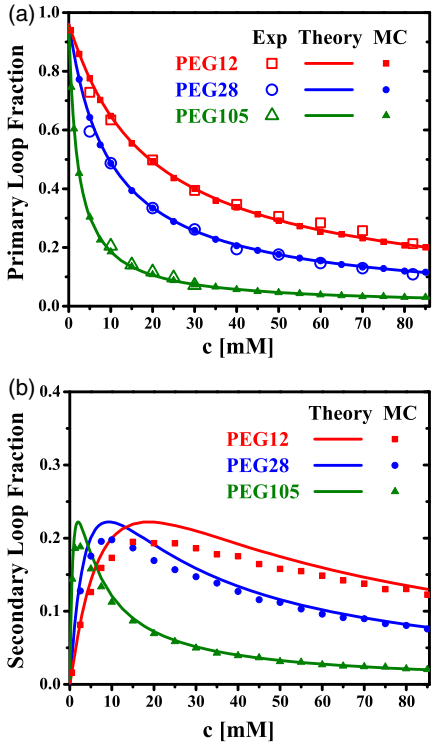

FIG. 2. (a) Primary loop fraction f_1 and (b) secondary loop fraction f_2 versus initial polymer molar concentration c calculated by the modified rate theory in comparison with the experimental data and MC simulation. In both the theory and simulation, the Kuhn length and molar mass of Kuhn monomer of PEG are chosen as $b = 1.1$ nm and $m = 137$g/mol [15].

variable characterizes the ratio between the intramolecular distance (edge connecting junctions within the same graph) and the intermolecular distance (edge between junctions in different graphs). When plotted against this dimensionless variable, f_n for different chain lengths in Fig. 2 collapse into master curves, as shown in Fig. 3(a), suggesting a superposition of the dilution effect and the chain-length effect, with the principle given by

$$f_n(M_2, c_2) = f_n(M_1, \alpha_M c_1), \tag{3}$$

where $\alpha_M = (M_1/M_2)^{3/2}$ is the shift factor for changing molar mass from M_1 to M_2. The experimental data for polymer precursors of different chain lengths span different regions along the master curve, joining together to form the entire "loop spectrum." The different scaling of c and M indicates that chain length is more effective in controlling loop fraction than concentration. The NDS experimental data shown in Fig. 2 are restricted to PEG networks; however, the master curves presented in Fig. 3(a) are universal for networks end-linked by all types of flexible polymers, given the corresponding Kuhn length and molar mass of Kuhn monomer. Therefore, this theory can be applied to a broad range of networks where the NDS technique is currently not applicable. While the exact form of the master curves depends on the functionality of junctions, the superposition principle for the dilution effect and chain-length effect revealed here is expected to demonstrate a universal property for all junction functionalities.

Besides the overall loop fraction, this theory also captures the short-range correlations between loops and ideal junctions, which provide insight on the spatial distribution of cyclic defects in networks. Based on the correlation between two primary loops, the entire loop spectrum can be divided into three regions [Fig. 3(b)]. In region 1, $f_{\text{tree}}/f_{\text{dumbbell}} < 10^{-3}$ [or $cb^3(M/m)^{3/2} < \sim 0.1$]; the tree structure that separates different loops is absent and primary loops are fully correlated (see Sec. III of Supplemental Material for the topological structure [41]): the network is sol. In region 3, $f_{\text{tree}}/f_{\text{dumbbell}} > 10^3$ [or $cb^3(M/m)^{3/2} > \sim 10$]; primary loops are rare, dumbbell primary loops (short-range correlations) disappear, and the tree structure dominates. The network (probably an elastomer or gel) is locally disturbed by loops without losing its long-range connectivity. Each primary loop is isolated, and the loop or bridge state of each chain is independent. Therefore, the gel can be envisioned as an "ideal loop gas." The impact of each loop on the network properties is linearly additive. Region 2 ($10^3 > f_{\text{tree}}/f_{\text{dumbbell}} > 10^{-3}$) is most accessible in experiment and meanwhile most complicated due to the coexistence of all species. Because of the saturation of junction functionality, the formation of different topologies is not

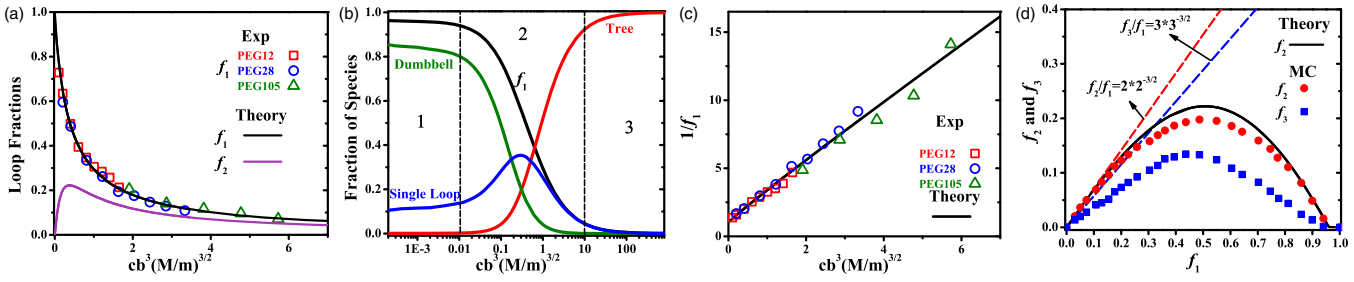

FIG. 3. Universal cyclic topology of polymer networks. (a) Master curves of primary and secondary loop fractions on the single dimensionless variable $cb^3(M/m)^{3/2}$ characterizing the network formation condition. (b) Plot of calculated fractions of different topological structures versus $cb^3(M/m)^{3/2}$ in the logarithm scale to illustrate three regions in the loop spectrum. (c) Linear relation between $1/f_1$ and $cb^3(M/m)^{3/2}$. (d) Loop diagram by plotting f_2 and f_3 versus f_1.

unconstrained but competitive, which is reflected by the nonmonotonic change in the fraction of single primary loops. Different cyclic defects weaken the network cooperatively in this region: the strands connecting two adjacent loops cannot be perceived as completely elastically active. Network properties depend on both the number of loops as well as their spatial arrangement.

Despite the presence of correlation between loops and ideal junctions in region 2, it is surprising that $1/f_1$ versus $cb^3(M/m)^{3/2}$ exhibits a linear relation [Fig. 3(c)], which leads to an analytical expression similar to the Langmuir adsorption isotherm as

$$f_1 = \frac{1}{1 + kcb^3(M/m)^{3/2}}, \tag{4}$$

with the coefficient k (slope of the line) depending on junction functionality. $f \approx [cb^3(M/m)^{3/2}]^{-1}$ as $cb^3(M/m)^{3/2} \gg 1$. This slow decay implies that achieving loop fractions close to zero is extremely difficult. The fact that primary loop fraction follows this mean-field-type description suggests some renormalization treatment of loops to remove the correlation.

Because the number of primary loops is a one-to-one function of $cb^3(M/m)^{3/2}$ and because all topologies depend solely on $cb^3(M/m)^{3/2}$, knowledge of the primary loop fraction is sufficient to determine the number of all higher-order topological structures in the network. This is illustrated as the "loop diagram" in Fig. 3(d). For very small f_1, where different loops are uncorrelated, f_2 and f_3 increase linearly, with the slope $f_n/f_1 = nn^{-3/2}$ in agreement with the intrinsic probability of closing Gaussian chains. With f_1 increasing, fractions of higher-order loops deviate downward from linearity, reaching a maximum and dropping to 0 as f_1 approaches 1. This strong nonmonotonic behavior indicates the competition in forming different loops due to the saturation of junction functionality. In particular, the existence of primary loops excludes the formation of higher-order loops. The maximum of f_3 appears at lower value of f_1 compared to the maximum of f_2, which indicates that the formation of the higher-order loop is more sensitive to the connectivity of its neighbor environment in the network. Furthermore, the fraction of higher-order loops is comparable to f_1, e.g., $f_2 + f_3 = 0.18$ as $f_1 = 0.2$; therefore, higher-order structures cannot be ignored. This explains why the network modulus observed in experiments cannot be described by only correcting for the primary loop effect [36,37].

Intuitively, one can envision many combinations of different topological defects (primary loops, secondary loops, etc.) that result in identical mechanical properties but varying primary loop fractions. However, results shown in Fig. 3(d) demonstrate that the relative populations of different topological defects are not freely adjustable; fractions of all higher-order loops are uniquely determined once f_1 is fixed. Statistically, there is one-to-one correspondence between network topology and primary loop fraction, universal for all flexible polymers. In other words, polymer networks can be uniquely categorized using the primary loop fraction, providing a more universal experimental observable to determine network topology than the variety of preparation conditions used in most previous studies. This categorization also facilitates directly mapping the cyclic defects in polymer network topology to the mechanical properties. Our results imply that any networks will have the same dimensionless modulus ($G/\nu kT$, where ν is the total density of polymer strands in the network) if they belong to the same loop category (same f_1). For the same monomer functionality ($A_2 + B_3$ in this work) and process for network synthesis, $G/\nu kT$ is uniquely determined once f_1 is fixed.

The two junction rate theory also facilitates the study of the loop formation kinetics during network formation. As shown in Fig. 4, the evolution of the primary loop fraction predicted by our theory is in excellent agreement with the NDS experimental data. Primary loops and secondary loops, generated from isolated intramolecular connection, are accumulated smoothly as conversion increases. On the contrary, the fraction of tree structures, related to the cooperative intermolecular connection, presents a sharp increase at higher conversion due to preferential formation of bridges. This can also be illustrated by the inset showing $f_{\text{tree}}/f_{\text{dumbbell}}$ and $f_{\text{tree}}/f_{\text{single loop}}$.) This sharp increase occurs at a conversion slightly larger than 0.7, the gel point of loop-free networks [1], which implies a global change of the network topology.

These results show the universal cyclic topology of polymer networks and its intrinsic dependence on the formation condition by studying flexible polymers end-linked via trifunctional junctions. Both the theory and conclusions can be generalized to more complicated polymer network systems with polydisperse chain length as well as other junction functionalities and chain statistics

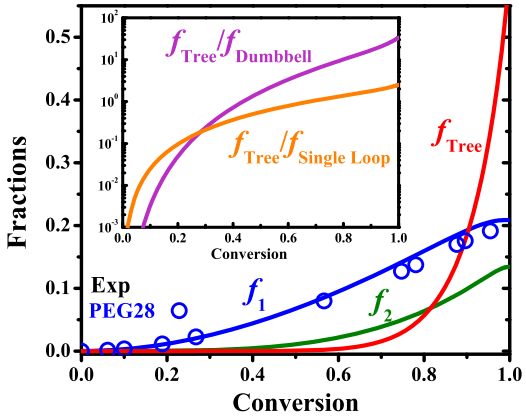

FIG. 4. Kinetics of loop formation. Fractions of primary loop, secondary loop, and tree structure versus conversion of functional groups in comparison with the NDS experimental data for PEG28 at $c = 40$ mM. The inset shows the ratios between the fractions of tree structure and dumbbell structure as well as the single primary loop structure, respectively.

(e.g., semiflexible polymers). The universal cyclic topology found in polymer networks is also anticipated to provide inspiration in the study of other types of networks, such as computer, biological, and social networks. The theory shows excellent agreement with the NDS experimental data without any fitting parameters, and can be applied to a broad range of networks where the NDS technique is currently not applicable. Quantifying different cyclic defects separately in this work enables decoupling their impacts, which is essential for developing correlations between topology and mechanical properties, an outstanding challenge in polymer science. Unifying the dilution and chain-length effects for network formation greatly reduces the parameter space experimentally available to tune network properties, providing a key step towards predictably designing the material properties by introducing the right amount of loops within polymer networks [46]. The universal relation between different cyclic defects indicates that different loop fractions cannot vary independently, in stark contrast to the intuition that arbitrary combinations of different loops can be synthesized. Once the primary loop fraction is known (which is now measurable in experiments), the polymer network topology is fully defined.

This work is supported by National Science Foundation (Award No. DMR-1253306). We thank Dr. Muzhou Wang for assistance in the Monte Carlo simulation.

*jaj2109@mit.edu
†bdolsen@mit.edu

[1] P. J. Flory, *Principles of Polymer Chemistry* (Cornell University Press, Ithaca, 1953).
[2] W. H. Stockmayer and L. L. Weil, in *High Polymers. Advancing Fronts in Chemistry*, edited by S. B. Twiss (Reinhold, New York, 1945).
[3] P. G. de Gennes, *Scaling Concepts in Polymer Physics*, 1st ed. (Cornell University Press, Ithaca, 1979).
[4] J. E. Mark and B. Erman, *Rubberlike Elasticity—A Molecular Primer* (Wiley, Chichester, 1988).
[5] K. Y. Lee and D. J. Mooney, Chem. Rev. **101**, 1869 (2001).
[6] X. X. Chen, M. A. Dam, K. Ono, A. Mal, H. Shen, S. R. Nutt, K. Sheran, and F. Wudl, Science **295**, 1698 (2002).
[7] M. P. Lutolf, J. L. Lauer-Fields, H. G. Schmoekel, A. T. Metters, F. E. Weber, G. B. Fields, and J. A. Hubbell, Proc. Natl. Acad. Sci. U.S.A. **100**, 5413 (2003).
[8] R. Langer and D. A. Tirrell, Nature (London) **428**, 487 (2004).
[9] D. E. Discher, D. J. Mooney, and P. W. Zandstra, Science **324**, 1673 (2009).
[10] Q. Wang, J. L. Mynar, M. Yoshida, E. Lee, M. Lee, K. Okuro, K. Kinbara, and T. Aida, Nature (London) **463**, 339 (2010).
[11] S. Lv, D. M. Dudek, Y. Cao, M. M. Balamurali, J. Gosline, and H. Li, Nature (London) **465**, 69 (2010).
[12] M. A. C. Stuart, Nat. Mater. **9**, 101 (2010).
[13] X. He, M. Aizenberg, O. Kuksenok, L. D. Zarzar, A. Shastri, A. C. Balazs, and J. Aizenberg, Nature (London) **487**, 214 (2012).
[14] J. Y. Sun, X. Zhao, W. R. K. Illeperuma, O. Chaudhuri, K. H. Oh, D. J. Mooney, J. J. Vlassak, and Z. Suo, Nature (London) **489**, 133 (2012).
[15] M. Rubinstein and R. H. Colby, *Polymer Physics* (Oxford University Press, Oxford, 2003).
[16] W. H. Stockmayer, J. Chem. Phys. **11**, 45 (1943).
[17] W. H. Stockmayer, J. Chem. Phys. **12**, 125 (1944).
[18] H. M. James and E. Guth, J. Chem. Phys. **21**, 1039 (1953).
[19] P. J. Flory, J. Chem. Phys. **66**, 5720 (1977).
[20] J. E. Mark and J. L. Sullivan, J. Chem. Phys. **66**, 1006 (1977).
[21] P. J. Flory, Polymer **20**, 1317 (1979).
[22] G. Hild, Prog. Polym. Sci. **23**, 1019 (1998).
[23] M. E. J. Newman, *Networks: An Introduction* (Oxford University Press, Oxford, 2010).
[24] R. Albert and A. L. Barabasi, Rev. Mod. Phys. **74**, 47 (2002).
[25] M. Gordon and S. B. Ross-Murphy, Pure Appl. Chem. **43**, 1 (1975).
[26] C. W. Macosko and D. R. Miller, Macromolecules **9**, 199 (1976).
[27] K. Dusek and V. Vojta, Br. Polym. J. **9**, 164 (1977).
[28] Z. Ahmad and R. F. T. Stepto, Colloid Polym. Sci. **258**, 663 (1980).
[29] S. Kuchanov, H. Slot, and A. Stroeks, Prog. Polym. Sci. **29**, 563 (2004).
[30] K. Suematsu, Adv. Polym. Sci. **156**, 137 (2002).
[31] F. Lange, K. Schwenke, M. Kurakazu, Y. Akagi, U. Chung, M. Lang, J. Sommer, T. Sakai, and K. S. Saalwachter, Macromolecules **44**, 9666 (2011).
[32] M. H. Samiullah, D. Reichert, T. Zinkevich, and J. Kressler, Macromolecules **46**, 6922 (2013).
[33] K. Saalwachter, M. Gottlieb, R. G. Liu, and M. Oppermann, Macromolecules **40**, 1555 (2007).
[34] H. Zhou, J. Woo, A. M. Cok, M. Wang, B. D. Olsen, and J. A. Johnson, Proc. Natl. Acad. Sci. U.S.A. **109**, 19119 (2012).
[35] H. Zhou, E. Schon, M. Wang, M. J. Glassman, J. Liu, M. Zhong, D. D. Diaz, B. D. Olsen, and J. A. Johnson, J. Am. Chem. Soc. **136**, 9464 (2014).
[36] Y. Akagi, J. P. Gong, U. Chung, and T. Sakai, Macromolecules **46**, 1035 (2013).
[37] M. Zhong, R. Wang, K. Kawamoto, B. D. Olsen, and J. A. Johnson (to be published).
[38] J. L. Stanford and R. F. T. Stepto, J. Chem. Soc. Faraday Trans. **71**, 1292 (1975).
[39] J. L. Stanford and R. F. T. Stepto, J. Chem. Soc. Faraday Trans. **71**, 1308 (1975).
[40] H. Rolfes and R. F. T. Stepto, Makromol. Chem. Makromol. Symp. **40**, 61 (1990).
[41] See Supplemental Material at http://link.aps.org/supplemental/10.1103/PhysRevLett.116.188302, which includes Refs. [34,35,42], for the list of subgraphs considered in the modified rate theory and the algorithm of Monte Carlo simulation.
[42] S. Dutton, R. F. T. Stepto, and D. J. R. Taylor, Angew. Makromol. Chem. **240**, 39 (1996).
[43] C. P. Broedersz and F. C. MacKintosh, Rev. Mod. Phys. **86**, 995 (2014).
[44] J. Wilhelm and E. Frey, Phys. Rev. Lett. **77**, 2581 (1996).
[45] Based on the chemical structure, the molar mass M of the three PEG precursors with repeating units 12, 28, and 105 are 1174 g/mol for PEG12, 1878 g/mol for PEG28, and 5266 g/mol for PEG105, respectively.
[46] A. C. Balazs, Nature (London) **493**, 172 (2013).